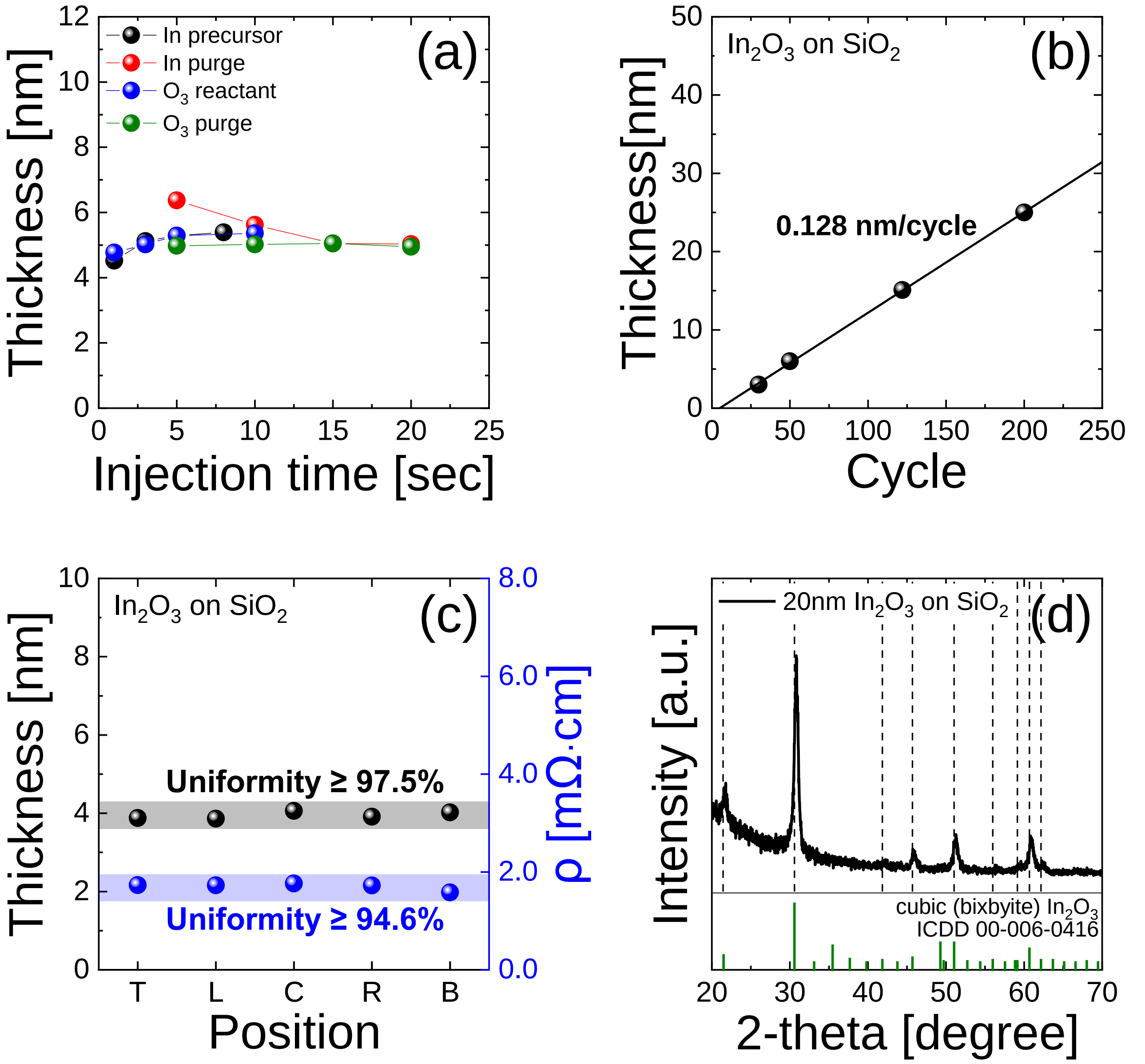

Fig. S1 (a) The saturation behavior of IO thin films as a function of precursor and reactant injection times. The film thickness remains nearly constant beyond a certain injection time (In precursor: 3 s, purge: 10 s, O_3: 5 s, purge: 5 s), indicating the saturation of the atomic layer deposition (ALD) process. (b) Linear relationship between film thickness and the number of ALD cycles, confirming a self-limiting and controlled growth mechanism of IO on SiO_2. (c) Thickness and electrical resistivity uniformity across different positions of the deposited IO films on SiO_2. The measured thickness variation indicates high uniformity, with values exceeding 97.5% measured by ellipsometry, while the resistivity uniformity is maintained above 94.6% measured by 4PP. (d) GIXRD data of a 20 nm-thick IO thin film grown on SiO_2, confirming the cubic bixbyite structure. The observed diffraction peaks match well with the standard reference pattern (ICDD 00-006-0416), indicating the crystalline nature of the deposited film.

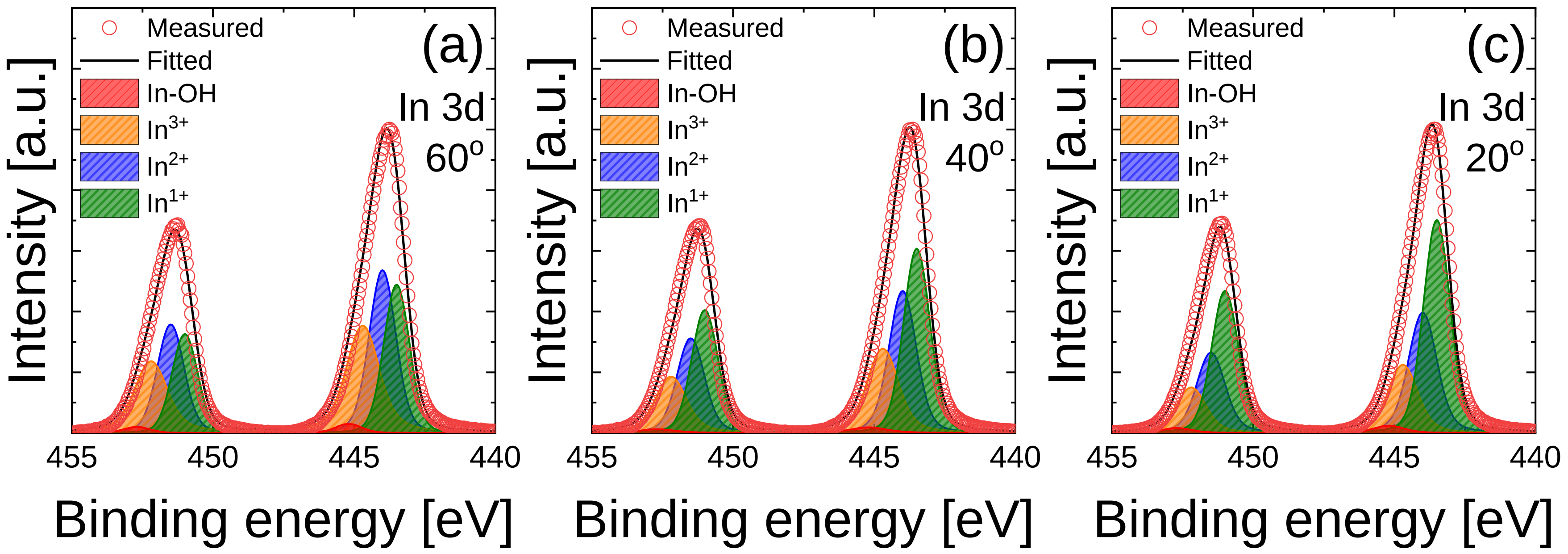

Fig. S2 In 3d ARXPS spectra of a 10 nm IO / 10 nm AO bilayer structure, measured at different stage angles: (a) 60°, (b) 40°, and (c) 20°. The measured spectra are fitted with contributions from different indium oxidation states. As the detection angle decreases the peak intensity corresponding to In^{3+} decreases, whereas the peaks corresponding to In^{1+} and In^{2+} increase.

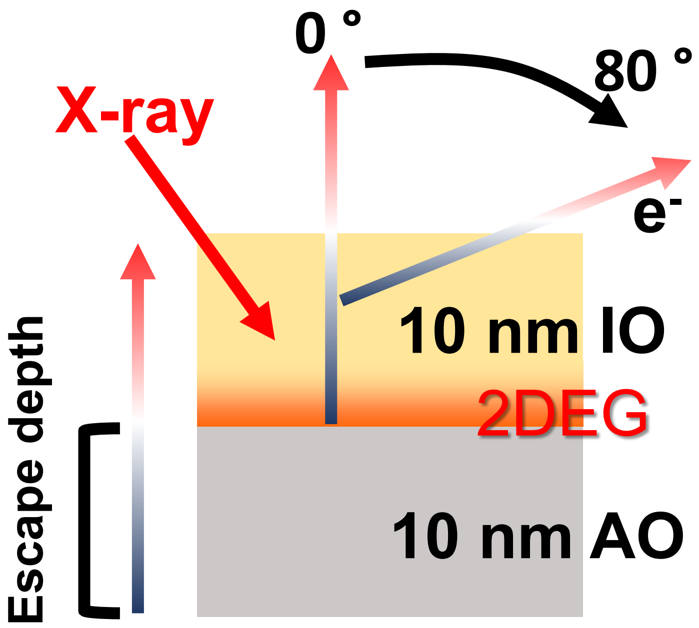

The equation is derived from the following assumptions:

(1) Photoelectron attenuation through the 10 nm-thick IO overlayer.

(2) The IO bulk is assumed to be stoichiometric

c : X-ray flux density
p : In^{1+-2+}/In^{3+} ratio in 2DEG layer
d : 2DEG thickness
λ_{IO} : Inelastic mean free path of photoelectrons in IO
t_{IO} : Total IO thickness (=10nm)

$$\frac{dI}{dt} = p\times c\times \exp\left(-\frac{t_{IO}-t}{\lambda cos\theta}\right)$$

$$I(In^{1+-2+}) = p\times c\times \int_0^{t_{IO}-d} \exp\left(-\frac{t_{IO}-t}{\lambda_{IO} cos\theta}\right) dt$$

$$= p\times I^{\infty}_{2DEG}\times \exp\left(-\frac{d}{\lambda_{IO} cos\theta}\right)\times\left[1-\exp\left(-\frac{t_{IO}-d}{\lambda_{IO} cos\theta}\right)\right]$$

$$I^{\infty}_{2DEG} = c\times\lambda\times\left(1-\exp\left(\frac{-t_{IO}}{\lambda_{IO} cos\theta}\right)\right)$$

$$I(In^{3+}) = I^{\infty}_{2DEG} - I(In^{1-2+})$$

$$\frac{I(In^{1+-2+})}{I(In^{3+})} = \frac{p\times \exp\left(-\frac{d}{\lambda_{IO} cos\theta}\right)\times\left[1-\exp\left(-\frac{t_{IO}-d}{\lambda_{IO} cos\theta}\right)\right]}{1-\exp\left(-\frac{t_{IO}}{\lambda_{IO} cos\theta}\right)-p\times \exp\left(-\frac{d}{\lambda_{IO} cos\theta}\right)\times\left[1-\exp\left(-\frac{t_{IO}-d}{\lambda_{IO} cos\theta}\right)\right]}$$

Fig. S3 An analytical model was newly adapted to quantitatively estimate the 2DEG thickness. This model uses the ratio of ARXPS intensities from the reduced In^{1+-2+} and fully oxidized (In^{3+}) states as a function of stage angle.

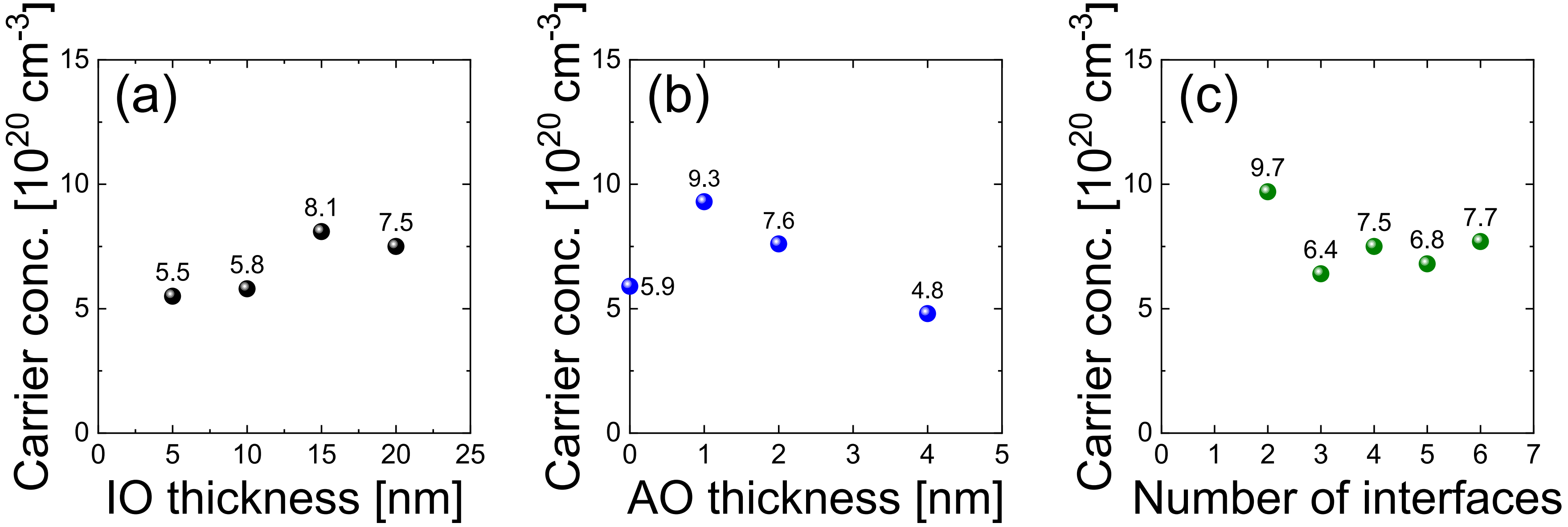

Fig. S4 Bulk carrier concentration of various ALD-structured AO/IO configurations as a function of (a) IO thickness, (b) AO thickness, (c) Number of interfaces. Except for the 4 nm AO sample, all NL structures exhibit higher carrier concentrations than bare IO, highlighting the beneficial role of AO layers and interface in improving carrier transport.